Combined role of regionegularity and molecular weight on meltcrystallization and self-nucleation of poly(3-hexylthiophene)

Ramin Hosseinabad, Jesse Kuebler, Lucia Fernandez-Ballester*

Department of Mechanical and Materials Engineering and Nebraska Center for Materials and Nanoscience, University of Nebraska at Lincoln, Lincoln, Nebraska 68588, United States.

* Corresponding author: Email: lucia.fernandez@unl.edu

Abstract

Melt-crystallization of conjugated polymers has potential as an environmentally-friendly alternative to solution processing, but the specific role of molecular attributes and potential control strategies remain largely unexplored. Here, two series of regioregular poly(3-hexylthiophene) (P3HT) reveal that the effects of chain length depend strongly on the amount of chain defects (regioregularity). Beyond the chain-folding transition, increasing molecular weight Mw for 90% regioregular P3HT results in slower crystallization kinetics and crystallites of reduced thermal stability, while 95% regioregularity renders crystallization nearly insensitive to chain length. Melt self-seeding can be used to manipulate the crystallization temperature of P3HT, but is most efficient when crystallization is hindered the most—i.e. for longer, more defective chains. P3HT self-seeding is dominated by the thermal stability of the crystallites originally present, and not by diffusion effects solely dependent on Mw. Overall, the results underscore the critical need to control and report both regioregularity and molecular weight.

Keywords: Poly(3-hexylthiophene), Melt-crystallization, Regionegularity, Molecular weight, Self-nucleation

1 Introduction

Conjugated polymers are currently the subject of much interest due to their optical and electrical conductivity properties, which make them candidates for applications such as flexible electronics, solar cells, light-emitting diodes and sensors [1-3]. A workhorse among this class of materials is regioregular poly(3-hexylthiophene) (P3HT), which has been widely explored in literature as a model conjugated semicrystalline polymer. Similarly to classical polymers, conjugated polymers exhibit strong relationships between their semicrystalline structure and final properties (conductive, mechanical, optical, etc.). For example, charge transport in P3HT is strongly influenced by a complex relationship between crystallinity, tie chains between crystalline aggregates, lamellar thickness, and long-range orientation [4-8]. In turn, the detailed semicrystalline morphology that forms in conjugated polymers is thought to depend strongly on the specific resin used and on the conditions under which crystallization occurs. However, the exact interplay between molecular attributes, processing conditions, and final structure is complex and remains elusive.

Solvent-free crystallization of P3HT—and of other conjugated semicrystalline polymers—has received much less attention than solution processing [5, 9-12]. Indeed, the vast majority of studies on P3HT involve the use of organic solvents, so crystallization occurs in solution [13-19].

While solvents afford relative ease of processing, melt-crystallization has potential as an environmentally-friendly alternative that does not require the use of toxic organic solvents, and crystallizing directly from the melt may result in structures not attainable through solution-crystallization. However, in order to envision potential use of melt-processing to yield optimal morphologies and properties in P3HT, the interplay between molecular variables (i.e. molecular weight, regioregularity, etc.), processing conditions, and crystallization must be understood and controlled.

The combined effect of molecular weight and regioregularity on crystallization of P3HT has not been explored, although each of these parameters has been examined individually while keeping the other approximately constant. When isolating the effect of chain length, most studies have examined P3HT samples in the lower molecular weight range which typically exhibit poor charge transport due to lack of connectivity between crystalline aggregates [4, 5, 20-22]. For such short P3HT chains—where chain-end effects are important and which may not yet be highly entangled—increasing molecular weight results in increasing melting temperature, crystallization temperature, and crystallinity [5, 11, 22-24]. Furthermore, below M_W ~ 19 kg/mol $(M_n \sim 11 \text{ kg/mol})$, the lamellar period increases with molecular weight and closely tracks the length of a fully extended chain, indicating extended-chain crystallization [25]. In contrast, fewer studies have explored the effect of chain length on crystallization of P3HT for molecular weights large enough that charge transport is no longer limited by crystalline connectivity, most relevant for applications. Indeed, increasing Mw quickly improves charge transport due to formation of tie chains, but beyond certain Mw tie chains cease to be limiting and transport within crystalline aggregates—weakly dependent on Mw-becomes the constraining factor. Above Mw ~ 19 kg/mol $(M_n \sim 11 \text{ kg/mol})$, the lamellar thickness saturates at $\sim 25 \text{ nm}$ indicating the onset of chain-folding [25], while levelling of melting and crystallization temperatures has been reported beyond M_w ~ $30 - 45 \text{ kg/mol} (M_n \sim 25 \text{ kg/mol}) [11, 24].$

The isolated effect of regio-defects on P3HT crystallization has been much less explored than molecular weight, despite the advent of synthetic innovations allowing control over regioregularity [26-29]. It is thought that regio-defects in the P3HT chain may either be excluded from the crystal or, if incorporated, result in an enthalpy penalty. Recently, Snyder *et al.* showed that more defective chains of P3HT yield thinner lamellae [30], while Luscombe demonstrated that regio-defects can be incorporated into the crystal lattice [31]. In general, studies which isolate the effect of regioregularity at fixed molecular weight find that higher regioregularity results in increasingly ordered morphologies and faster charge transport [32-36]. However, the combined role of regioregularity and molecular weight on P3HT crystallization has not been examined.

In contrast to conjugated polymers, the role of molecular weight and chain defect content on crystallization and melting of classical polymers has been extensively investigated over a wide range of molecular weights [37-40]. For very low molecular weights where chain end effects are still important, melting and crystallization temperatures increase with increasing molecular weight. As the molecular weight becomes large enough that chain end effects no longer dominate, the behavior changes: linear homopolymers generally exhibit a plateau and then slight decrease in their crystallization temperature along with nearly invariant melting temperatures,

while random copolymers or branched polymers show a clear decrease in both crystallization and melting temperatures with increasing chain length [37-39, 41].

Even though the crystallization process plays a key role on final morphology and properties, strategies to control crystallization of conjugated polymers are limited—particularly for solvent-free processing. Self-nucleation (SN) is a technique for control of nucleation first described by Keller that consists of dissolving or melting selected crystalline populations to yield either small crystal fragments or polymer chain bundles with residual segmental orientation, which can subsequently act as "seeds" or "self-nuclei" from which crystallization ensues [42-44]. The resulting increase in number of nuclei/volume yields increased crystallization temperatures, faster kinetics, and changes in semicrystalline morphology [43]. SN has been widely applied to traditional polymers, but there are few examples of SN in conjugated polymers and most are in the presence of solvents [13, 45-47]. Solvent-free SN has rarely been applied to P3HT and was found to be ineffective for particular P3HT grades, attributed to relatively high densities of nuclei/volume in P3HT [48-50]. However, it is unknown whether the effectiveness of a SN protocols remains limited across P3HT melts of various regioregularities and molecular weights.

In this study, we investigate the combined role of chain defects (regioregularity) and chain length (M_W) on the process of melt-crystallization of P3HT. The used molecular weights are large enough that chain-folded crystallization and significant chain entanglement is expected, and the examined regioregularities are relatively high (\geq 90%). Then, we examine the self-nucleation behavior of P3HT and its effectiveness in manipulating the crystallization process and increasing crystallization temperature across a range of chain molecular characteristics.

2 Experimental

2.1 Materials

Two series of poly(3-hexylthiophene) (P3HT) of varying molecular weights were obtained from Rieke Metals and used without further purification (Table 1). Each series had matched regioregularities of either $^{\sim}$ 90% (named "R90" series hereafter) or $^{\sim}$ 95% ("R95" series). Each sample name reflects the corresponding series and the weight-averaged molecular weight M_w . Characterization data from GPC and 1 H NMR is provided in Figure S1 and S2 in Supplementary Data.

| Series | Sample | $M_{\rm w}$ | M _n | PDI | rr |
|----------|---------|-------------|----------------|-----|-----|
| | | (kg/mol) | (kg/mol) | | (%) |
| R90-P3HT | R90-25k | 25.0 | 14.4 | 1.7 | 91 |
| | R90-46k | 46.1 | 20.5 | 2.2 | 90 |
| | R90-66k | 66.4 | 27.6 | 2.4 | 90 |
| | R90-79k | 78.7 | 35.1 | 2.2 | 89 |
| | R90-91k | 91.3 | 37.5 | 2.4 | 90 |
| R95-P3HT | R95-29k | 29.3 | 14.6 | 2.0 | 95 |
| | R95-40k | 40.4 | 19.3 | 2.1 | 95 |
| | R95-55k | 55.2 | 23.7 | 2.3 | 95 |
| | R95-83k | 83.4 | 37.1 | 2.2 | 96 |

Table 1. Molecular characteristics of R90 and R95 series. M_W : weight-average molecular weight, M_n : number-average molecular weight, PDI: polydispersity index, rr: regionegularity.

2.2 Differential Scanning Calorimetry (DSC)

Samples of approximately 3-4 mg of P3HT were punched from a press-molded film, placed inside a Tzero aluminum pan-lid assembly, and crimped with a T-zero press. Care was taken to ensure that the sample had optimal contact with the bottom of the pan. DSC measurements were performed with a TA Instruments Q250 differential scanning calorimeter under nitrogen atmosphere. Prior to non-isothermal and self-nucleation experiments, each sample was thermally erased to remove previous history. The heating and cooling rates were fixed at 10 °C/min for both non-isothermal and self-nucleation experiments.

2.2.1 Non-isothermal (NI) experiments

The thermal protocol for non-isothermal crystallization/melting experiments consisted of heating to T_e = 260 °C, isothermally holding for 5 min, cooling to 100 °C and holding for 1 min, and then heating again to 260 °C. Data was analyzed using TA Instruments TRIOS software to obtain peak crystallization and melting temperatures (T_c and T_m), and melting enthalpies (ΔH_m).

2.2.2 Self-nucleation (SN) experiments

The self-nucleation (SN) thermal protocol consists of alternating "non-isothermal cycles" (non-shaded segments in Figure 1) and " T_S -cycles" (shaded segments in Figure 1). First, the polymer was heated to an erasing temperature $T_e = 260\,^{\circ}\text{C}$, held isothermally for 5 min, and then cooled to 100 °C where it was allowed to stabilize for 1 min. At this point, a "standard state" of the sample had been created. The polymer was then heated to a pre-selected holding temperature T_S and held isothermally for 5 min. Next, the sample was cooled to 100 °C (shaded cooling ramp), stabilized for 1 min, and then heated to T_e again (shaded heating ramp). Afterwards, alternating non-isothermal and T_S —cycles with varying values of T_S were performed.

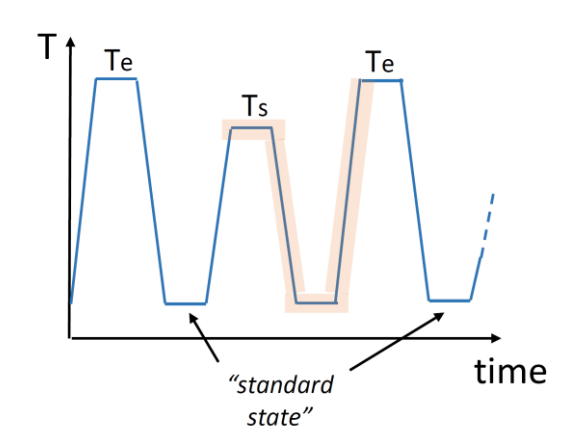


Figure 1. Thermal protocol for self-nucleation experiments.

The crystallization trace after holding at T_S as well as the subsequent melting trace (shaded cooling and heating ramps in Figure 1, respectively) were analyzed with TA instruments TRIOS software to extract crystallization and melting temperatures as well as melting enthalpies. The results served to determine whether a particular value of T_S resulted in the desired *self*-

nucleation domain (Domain II). From higher to lower T_S, three possible domains of behavior were described by Fillon as follows [43]:

- *Domain I or full melting domain*: subsequent crystallization and melting are unchanged when compared to a non-isothermal cycle.
- Domain II or self-nucleation domain: some self-nuclei survive the partial melting process at T_S, so subsequent crystallization occurs at higher temperatures due to the increased number of nuclei.
- Domain III or annealing domain: some crystallites anneal at T_S, resulting in an extra high temperature endothermic peak in the subsequent heating. Upon cooling from T_S, a high temperature exothermic shoulder or peak may emerge, attributed to recrystallization.

Recently, further subdivision of the *self-nucleation Domain II* has been proposed: *self-seeding Domain IIb*, when T_S is low enough for some crystal fragments or self-seeds to survive—i.e. $T_S < T_{m,end}$ of the DSC melting endotherm—and *melt-memory Domain IIa*, for T_S is well above the melting endotherm such that only non-crystalline self-nuclei could survive [51].

2.2.3 X-ray diffraction

Ex-situ transmission X-ray diffraction was performed at the 12-ID-B beamline at the Advanced Photon Source (Argonne National Laboratory) using incident x-rays with energy 13.30 keV. 2D scattering patterns were simultaneously collected on two detectors (a Pilatus 300k and a Pilatus 2M mounted $^{\sim}$ 0.4 and 2.0 m from the sample, respectively) to cover the desired q-range. An exposure time of 1 s was used. The 2D patterns were radially averaged and stitched to produce 1D intensity vs. q plots.

3 Results and discussion

Thermal properties.

3.1 Role of regioregularity and molecular weight on melt-crystallization

The effect of molecular weight M_W on P3HT non-isothermal crystallization and melting temperatures (T_c and T_m respectively) is strongly dependent on chain defect content, exhibiting very different trends for 90% and 95% regioregularity. On one hand, T_m and T_c for R95 samples do not significantly vary with M_W and the crystallization peak remains sharp, nearly unchanged for all samples (Figure 2a,b). In stark contrast, the lower regioregularity R90 series exhibits a clear decrease in both T_m and T_c with increasing M_W (Figure 2c,d), and the crystallization peak progressively broadens with increasing chain M_W . For 90% regioregular P3HT, the decrease in T_c is more pronounced than that of T_m . A small high temperature shoulder is observed during melting of all R90-P3HT samples as well as for R95-29k; it is possible that some melting-recrystallization process may occur during heating.

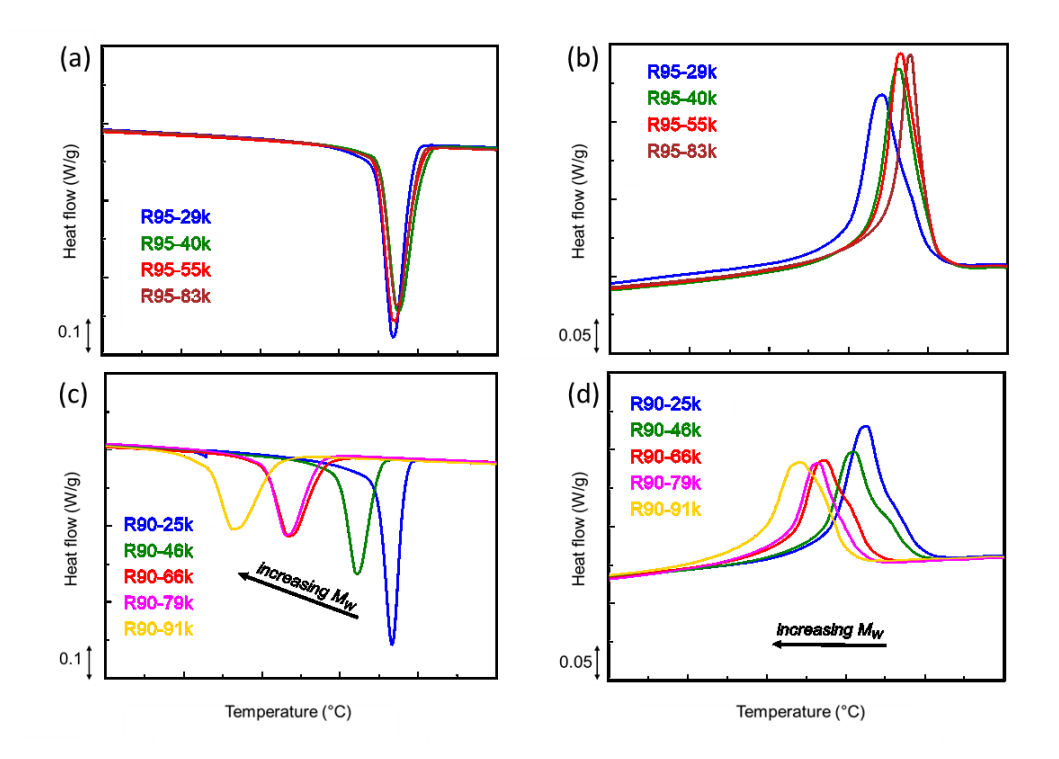


Figure 2. DSC traces for samples of varying M_W during (a) cooling of P3HT-R95; (b) heating of P3HT-R90; (d) heating of P3HT-R90.

The results above indicate that crystallization kinetics and thermal stability of the resulting crystallites are strongly dependent on both chain length and chain defect content, with just a 5% difference in regioregularity leading to significantly different behaviors. Indeed, the strong decrease in T_c and T_m with increasing M_W reveals that longer chains of 90% regioregularity experience increasingly sluggish crystallization kinetics and progressively reduced crystalline stability, while P3HT with \sim 5% higher regioregularity exhibits crystallization kinetics and thermal stability that are nearly insensitive to chain length (Figure 3a-b).

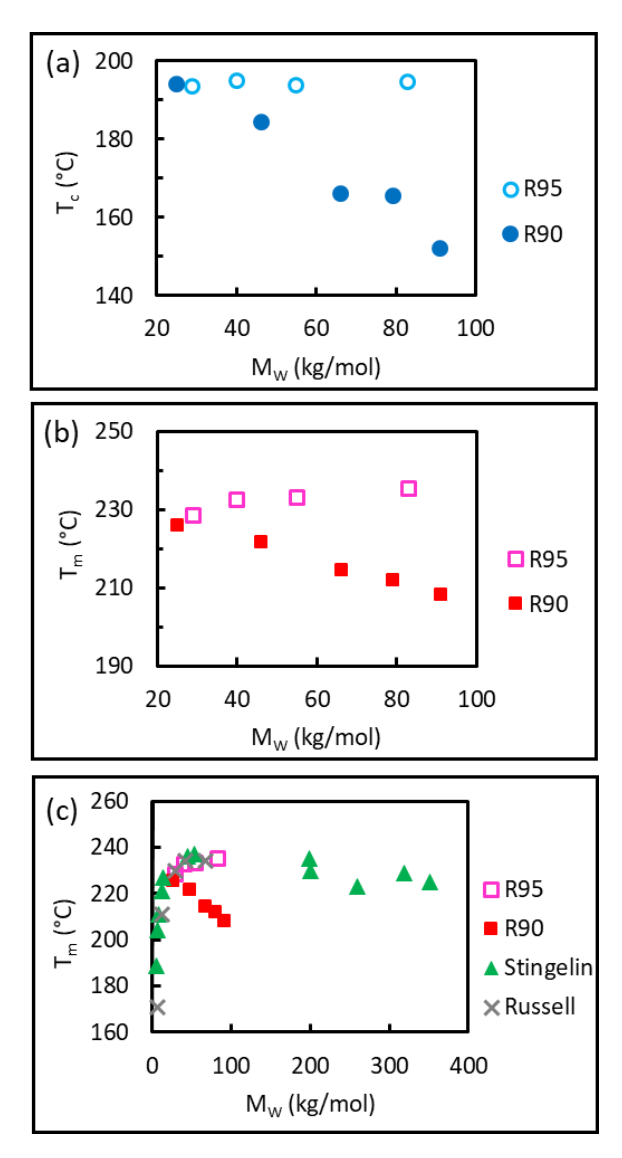


Figure 3. Effect of M_W on (a) crystallization and (b) melting temperature for R90-P3HT and R95-P3HT. (c) Comparison of non-isothermal T_m for P3HT-R90 and P3HT-R95 with T_m reported in previous studies for melt-crystallized samples where literature data has been replotted in terms of M_W (adapted with permission from [24] copyright 2014 American Chemical Society and from [11] copyright 2013 Elsevier).

The steep reduction in T_c and T_m with increasing M_w for 90% regioregular P3HT can be qualitatively explained in terms of the need to select crystallizable chain segments combined with the increasing sluggishness of longer chains. P3HT of lower regioregularity has a larger proportion of defects and, thus, smaller availability of chain segments between defects that are long enough (i.e. "crystallizable") to be incorporated into a crystal. Therefore, there is higher probability that a crystallizable chain segment may not be available near the growing crystal. When that occurs, crystallization will only proceed when a long enough crystallizable chain segment diffuses to the growth front. In samples of higher M_w , the longer polymer chains are increasingly entangled so diffusion of crystallizable chain segments to the growth front is expected to be more sluggish (Figure 4b), resulting in a slower, hindered crystallization process that occurs at lower

temperatures and yields thinner crystallites of lower thermal stability. Conversely, faster diffusion in lower M_w P3HT can provide adequate supply of crystallizable segments to the growth front (Figure 4a).

In contrast, the selection and transport process of crystallizable chain segments does not significantly hamper crystallization of 95% regioregular P3HT, even for the longest chains with $M_w = 83$ kg/mol. The molecular weight range probed for the R90 and R95 series is similar, so their chain dynamics should be comparable. Thus, the increasingly sluggish diffusion process of longer 95% regioregular chains is not a limiting factor for crystallization, likely due to the presence of enough available crystallizable segments near the crystalline growth front. In other words, because R95-P3HT has less chain defects than R90-P3HT, there is a larger pool of crystallizable sequences, increasing the probability that crystallizable chain segments are available near the growth front (Figure 4c, d) and thus leading to adequate supply of suitable chain segments to the growth front during crystallization regardless of molecular weight (i.e. of diffusion rate).

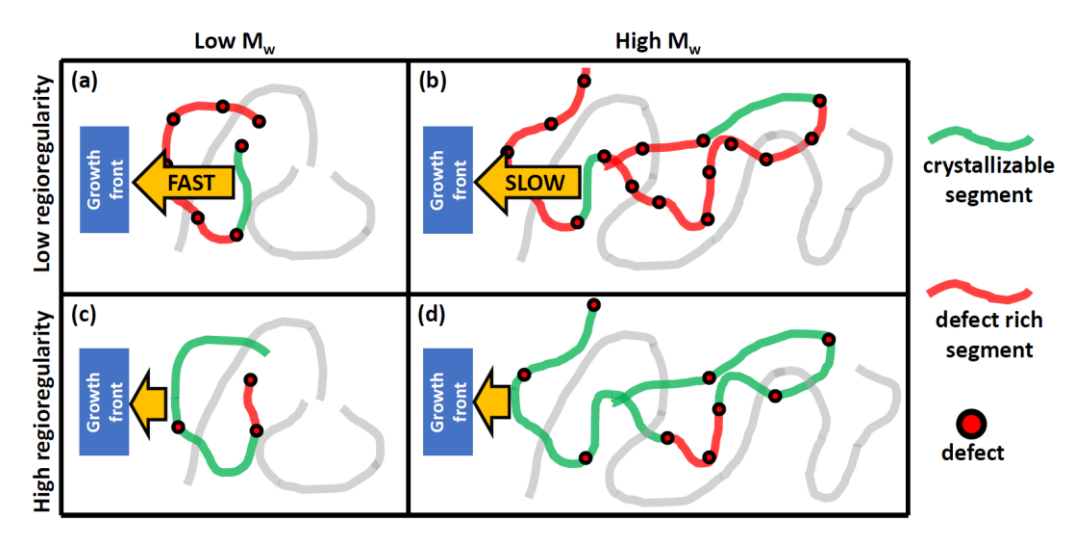


Figure 4. Schematic depicting transport of crystallizable chain segments to the growth front for P3HT of different molecular weights and regionegularities. Crystallizing chain is depicted in green (crystallizable segments) and red (defect-rich segments). Other chains in the melt are depicted in grey.

Interestingly, the T_c and T_m for the R90 and R95 series become progressively similar as M_W decreases, (Figure 3a-b), indicating that crystallization kinetics and crystallite thermal stability become increasingly comparable despite the 5% difference in regionegularity. In other words, faster chain diffusion in R90-P3HT of decreasing M_W increasingly enables adequate supply of crystallizable segments to the growth front, so the behavior of shorter 90% regionegular chains approaches that of their 95% counterparts. Likewise, as M_W increases, the behavior of the R90 and R95 P3HT progressively diverges: for example, $M_W \approx 80$ kg/mol, 95% regionegular P3HT crystallizes ≈ 29 °C and melts ≈ 23 °C higher than 90% regionegular P3HT. It should be noted that, while molecular weight distribution can exert some influence on thermal properties, the P3HT samples in this study have similar polydispersity indices. Furthermore, because the crystallization and melting behavior is inferred from the overall trend across a wide range of molecular weights

in each series, any effects arising from small differences in molecular weight distribution are expected to be negligible.

The few studies that examine molecular weights well beyond the chain folding transition report behavior matching that of R95-P3HT, i.e. nearly constant T_m above $M_w \sim 30$ kg/mol (Figure 3c). Clearly, the M_w range of the R95 series corresponds to the beginning of a plateau in T_m ; furthermore, T_m of R95 samples closely matches the melting temperatures reported by Russell (94-96% regioregular P3HT) and Stingelin (P3HT of matched but unreported regioregularity) [11, 24]. In contrast, the behavior of R90-P3HT strongly diverges, and the resulting thermal stability strongly decreases for longer chains (filled squares in Figure 3c). The disparate effect of M_w for R90 and R95-P3HT highlights the key role of regioregularity on melt-crystallization and underscores the need to account for chain defect content.

Melting enthalpies (ΔH_m) are impacted by both molecular weight and regioregularity, and vary between ~ 19 - 11 J/g for R90-P3HT and 21 - 17 J/g for R95-P3HT (Figure 5). Both series exhibit a decrease in ΔH_m with increasing M_w , which indicates that longer chain lengths somewhat hinder the overall ability to crystallize at fixed regioregularity and is attributed to the accompanying increase in chain entanglements. For fixed molecular weight, the ΔH_m is always smaller for 90% regioregularity, indicating that a larger amount of chain defects results in lower attainable crystallinity for comparable chain lengths.

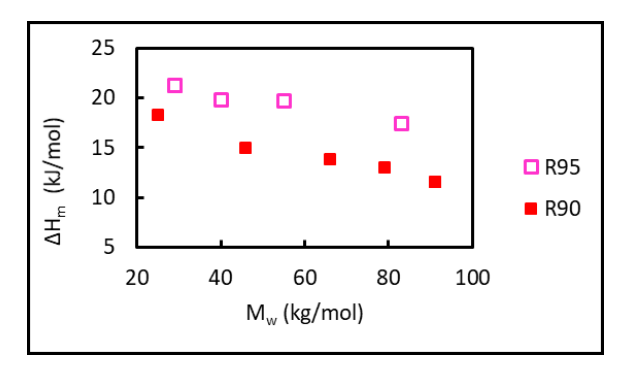


Figure 5. Melting enthalpy after non-isothermal crystallization vs. M_W for samples with 95% RR (empty squares) and with 90% RR (filled squares).

Crystallinity and lamellar thickness.

Crystallinity (X_C) may be extracted from the experimental ΔH_m by dividing by ΔH_m^{∞} , the heat of fusion of a perfect crystalline structure of *form I* P3HT. The specific value of ΔH_m^{∞} remains the subject of discussion: 33 – 99 J/g have been reported, and recent studies favor values between 33 - 49 J/g [9, 48, 52-54]. Using ΔH_m^{∞} = 49 J/g, a lower bound for crystallinities can be estimated: with increasing M_w, X_C for R95-P3HT decreases from ~ 43 to 36% while X_C for R90-P3HT decreases from 37 to 24%.

All non-isothermally crystallized samples—irrespective of molecular weight and regionegularity—exhibit transmission WAXD patterns with isotropic rings for both (100) and (020) reflections, indicating that there is no overall preferential orientation on the plane of the film (Figure S3 in Supplementary Data). The interplanar distance in the alkyl-chain stacking direction

 $d_{(100)} \sim 1.66$ nm is consistent with *form I* of P3HT [23] and does not significantly vary with chain length or regiodefect content; likewise, pi-pi stacking distance is $d_{(020)} \sim 0.38$ nm for all samples (Figure 6). Therefore, the dimensions of the crystalline unit cell are invariant for the range of chain lengths and defect content examined in this study.

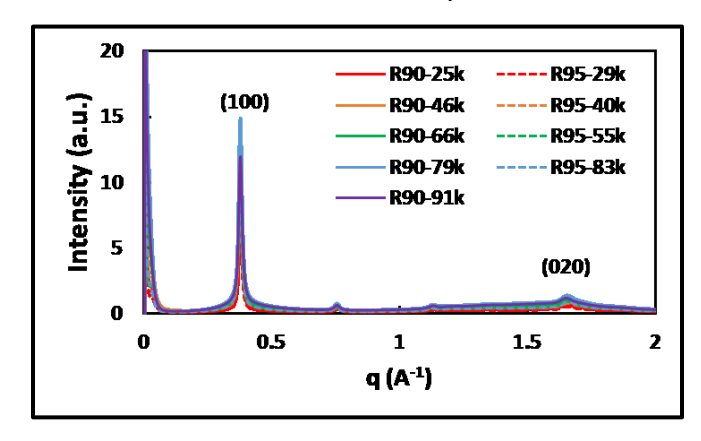


Figure 6. XRD patterns of R90 and R95 series after non-isothermal crystallization.

Lamellar thickness I_C generally correlates well with melting temperature of polymers, and the Gibbs-Thompson expression has been widely used to describe the decrease in T_m due to finite crystallite thickness [55]. However, Gibbs-Thompson does not take into account the presence of chain defects: as described by the Sanchez-Eby theory, partial inclusion of chain defects in the crystalline phase can additionally decrease melting temperature through an enthalpic penalty [56, 57]. In the current study, the melting temperatures of R90-25k and R95-29k are similar in spite of their disparate defect content, suggesting that the proportion of defect inclusion in the crystals is not dramatically different for 90% and 95% regioregular P3HT and that the trends in T_m with M_w are likely dominated by I_c . Consequently, it may be inferred that crystalline thickness of 95% regioregular P3HT does not significantly vary with M_w , while I_c of 90% regioregular P3HT decreases with increasing chain length.

Comparison with classical polymers.

The combined effect of molecular weight and regioregularity on melt-crystallization of P3HT, exhibits similarities with the behavior reported for classical polymers—such as polyethylene—of various chain lengths, defect content, and defect types (such as branching or copolymerization). For example, the non-isothermal crystallization behavior of R95-P3HT samples is similar to that of classical linear polymers and homopolymers; likewise, R90-P3HT resembles that of classical copolymers and branched polymers (for molecular weights large enough to render chain-end effects negligible). Indeed, increasing Mw results in only small variations in Tm for polyethylene homopolymers, while random ethylene copolymers exhibit a clear decrease in Tm attributed to kinetic constraints during crystallization due to the selection and transport process of crystallizable chain segments [37, 38, 41]. Likewise, increasing Mw in linear polyethylene results in a plateau and slight decrease of Tc and nearly constant Tm, while low density polyethylene exhibits a clear decrease in Tc and Tm attributed to the presence of short-chain branches [39]. Therefore, R95-P3HT is deemed to have a small enough amount of defects that allow it to behave similarly to a classical homopolymer or linear polymer (at least under the crystallization

conditions used in this study), while the greater quantity of chain defects in R90-P3HT renders its behavior similar to a copolymer or a branched polymer. Indeed, P3HT with regio-defects is thought to effectively behave as a copolymer [30].

The decrease in crystallinity with increasing P3HT chain length—regardless of content defect—has also been observed in both polyethylene homopolymers and copolymers at moderate molecular weights, prior to plateauing at very high molecular weights [37, 40, 58]. Likewise, an increase in percentage of chain defects in polyethylene copolymers at fixed M_W correlates with a decrease in crystallinity [37].

3.2 Crystallization through self-nucleation

Upon application of a self-nucleation protocol, all P3HT samples exhibited the typical *Domain I* (melting), *Domain II* (self-nucleation), and *Domain III* (annealing), although the range of T_s for each domain and the maximum attainable crystallization temperature varied across samples. In Figure 7a, the set of crystallization exotherms obtained for R90-66k when cooling from various T_s is displayed as a representative example of the self-nucleation behavior. For the highest holding temperatures ($T_s \ge 233$ °C), the ensuing crystallization process is indistinguishable from non-isothermal crystallization (compare red vs. black in Figure 7a), indicating that full melting was attained (*Domain II*). Upon further decrease of T_s (225 °C $\le T_s \le 232$ °C), the self-nucleation *Domain III* is reached (green traces) and T_c starts shifting to higher temperatures. Finally, the annealing *Domain III* (blue traces) is attained at $T_s = 224$ °C when a high temperature endothermic peak emerges in the melting trace (black arrow in Figure 7b) revealing that some annealing of crystallites occurred at the holding temperature T_s , while a small high temperature shoulder—due to recrystallization typical of Domain III—starts emerging during cooling in addition to the self-nucleation crystallization peak.

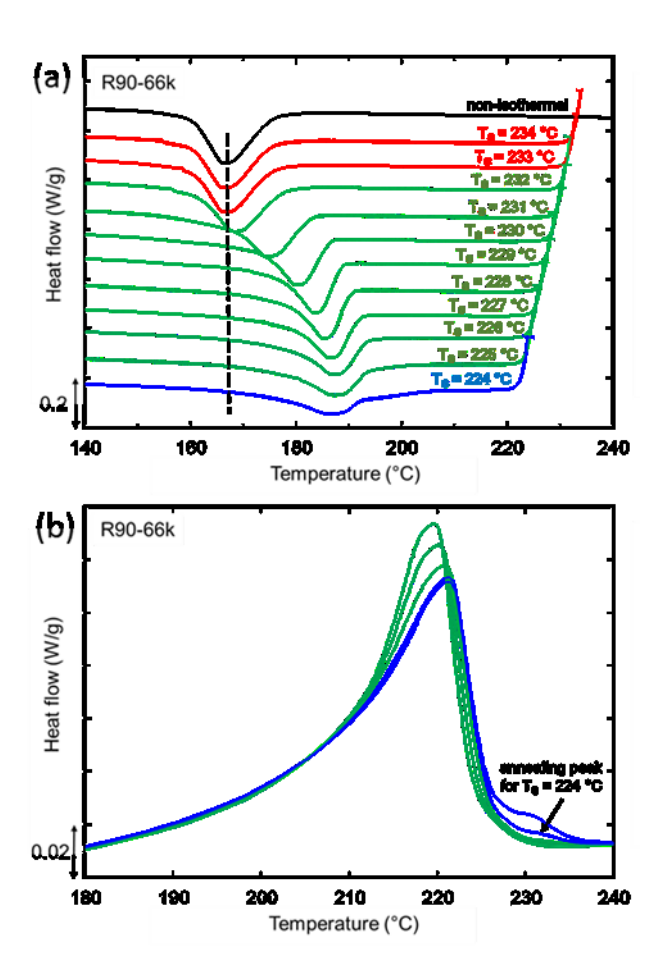


Figure 7. (a) DSC crystallization exotherms for non-isothermal cycle (black), and for cooling after $T_S = 234 - 224$ °C (red for Domain I, green for Domain II, blue for Domain III). (b) Melting endotherms after cooling from $T_S = 226 - 225$ °C (green, Domain II) and $T_S = 224 - 223$ °C (blue, Domain III). Emergence of an annealing peak for $T_S = 224$ °C is indicated with an arrow.

The maximum attainable self-nucleation crystallization temperature $T_{C,MAX}$ for all samples occurred for the lowest holding temperatures T_s in *Domain II* —i.e. near the boundary between *Domains II* and *III*)—through a self-seeding (SS) process, in the absence of detectable annealing of crystallites. A representative example is shown in Figure 8, where the peak crystallization temperature attained due to self-seeding for R90-66k (filled circles) is plotted against T_s and superimposed with its non-isothermal melting endotherm (solid line). Clearly, *Domain II* occurs near—but still within—the end of the non-isothermal melting trace, indicating that the increase in T_c is caused by residual crystallite fragments (self-seeds) and not by melt-memory effects arising from self-nuclei well above the melting endotherm. The width in T_s of Domain II was similar across the P3HT samples, ranging between $T_s = 10^{\circ}$ C. Upon decreasing $T_s = 10^{\circ}$ C first increases, then plateaus reaching the maximum attainable T_{C-MAX} near the domain boundary, and finally starts decreasing once *Domain III* is reached. A plateau in T_c at the lower end of *Domain II* has been observed in other polymers and attributed to reaching a critical nucleation density ($T_s = 10^{\circ}$ C and $T_s = 10^{\circ}$ C are incleased in nucleation density does not result in significant shift of the calorimetrically measured $T_c = 10^{\circ}$ C and $T_s = 10^{\circ}$ C are incleased in nucleation density does not result in significant shift of the calorimetrically measured $T_c = 10^{\circ}$ C and $T_s = 10^{\circ}$ C are incleased and $T_s = 10^{\circ}$ C and $T_s = 10^{\circ}$ C are incleased and $T_s = 10^{\circ}$ C and $T_s = 10^{\circ}$ C are incleased and $T_s = 10^{\circ}$ C and $T_s = 10^{\circ}$ C are incleased a

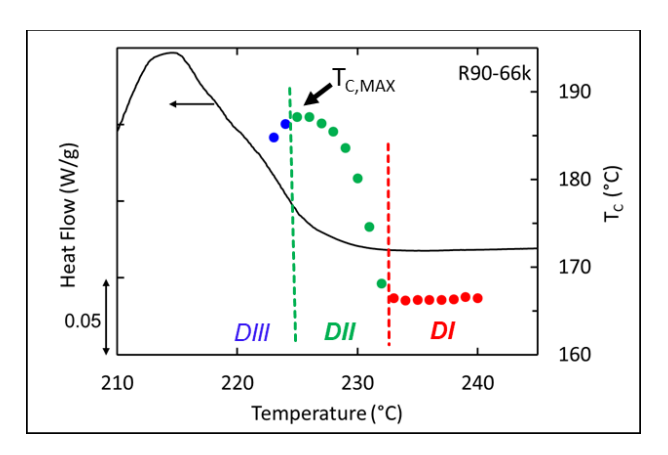


Figure 8. Peak crystallization temperature due to self-seeding for each T_s (circles) and non-isothermal melting trace (solid line) for R90-66k. Vertical dashed lines separate Domains I, II, and III. The maximum crystallization temperature attainable through self-seeding ($T_{C,MAX}$) is indicated with an arrow.

3.3 Role of regioregularity and M_W on effectiveness of self-seeding

Although the crystallization temperature can be manipulated through self-seeding in all P3HT samples, the maximum attainable $T_{C,MAX}$ as well as the relative increase in T_C of each specimen were strongly dependent on regioregularity and M_W . The R90 series exhibited a strong dependence of T_C with M_W , with samples of lower molecular weight reaching higher crystallization temperatures than those with longer chains (Figure 9a). In contrast, the 95% regioregularity series did not exhibit much change in T_C across different molecular weights (Figure 9b). Likewise, the holding temperature T_S needed to attain the maximum crystallization temperature was nearly invariant with M_W for R95-P3HT but decreased strongly with increasing chain length for R90-P3HT, indicating that the boundary between *Domain II* and *Domain III* was nearly fixed for 95% regioregular P3HT but occurs at progressively lower T_S for longer 90% regioregular chains. Similarly, the transition from Domain I to Domain II—evident by the sudden increase in T_C with decreasing T_S in Figure 9—occurs at similar T_S for all R95-P3HT samples but at decreasing T_S with increasing M_W for R90-P3HT.

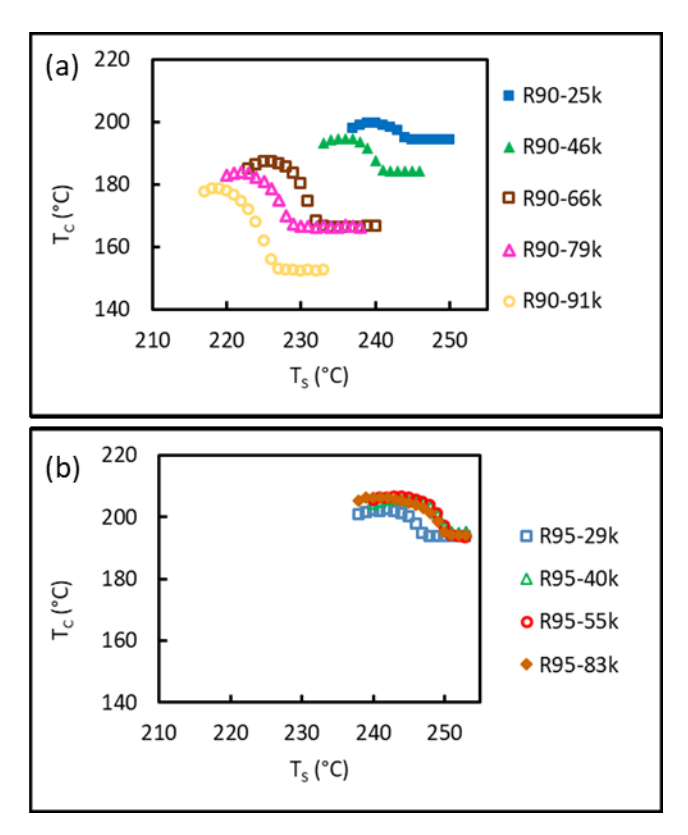


Figure 9. Effect of T_S on the crystallization temperature attainable by self-seeding T_C for (a) 90% regionegular and (b) 95% regionegular P3HT.

Although self-seeding increased the crystallization temperature in all P3HT samples, it was found to be most effective for P3HT of lower regioregularity and higher M_W —i.e. it produced the highest relative increase in T_C . The maximum attainable crystallization temperature $T_{C,MAX}$ was extracted from Figure 9 and compared with the non-isothermal T_C of each sample in Figure 10, where the shaded area corresponds to the maximum possible increase in crystallization temperature due to self-seeding ($\Delta T_{C,MAX}$). The largest increase $\Delta T_{C,MAX} \sim 26$ °C occurred for R90-91k P3HT, that is, the longest and most defective chains. As the molecular weight of 90% regioregular P3HT is decreased, $\Delta T_{C,MAX}$ becomes progressively smaller until it reaches ~ 5 °C for R90-25k. In contrast, the series with higher 95% regioregularity exhibits a relative increase in T_C of ~ 9 -13 °C, almost invariant with M_W .

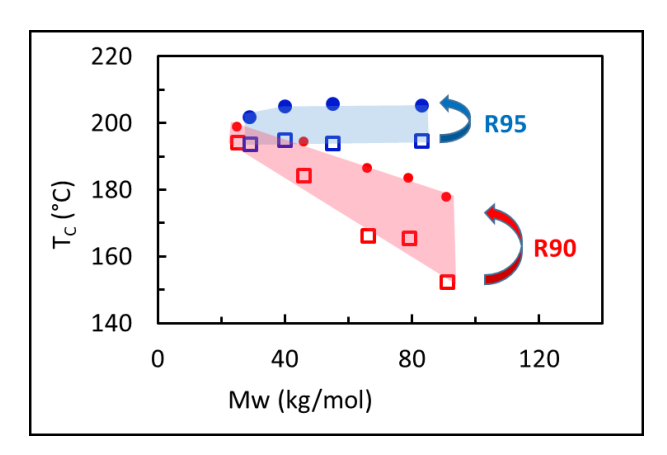


Figure 10. $T_{C,MAX}$ attainable by self-seeding (filled circles) and non-isothermal T_c (empty squares) vs. M_W for 90% regionegularity (red) and 95% regionegularity (blue). The shaded areas represent the maximum relative increase in crystallization temperature $\Delta T_{C,MAX}$.

The results above reveal that the impact of self-seeding on P3HT melt-crystallization depends strongly on both chain length and amount of chain defects. Self-nucleation most effectively increases T_C for P3HT samples with lowest regionegularity and highest M_W : in other words, SN causes the largest rise in T_C in samples for which the process of crystallization was hindered the most. The magnitude of the increase in T_C of polymers through self-nucleation is thought to depend not only on the relative increase in nuclei number-density but also on the temperature dependence of the linear growth rate [60]; whether one of these two factors dominates the large ΔT_C observed in longer, more defective P3HT chains in this study remains an open question.

To date, few studies have used self-nucleation in P3HT so its potential remains largely untapped. It was previously considered that self-nucleation protocols are not particularly influential in P3HT samples with ~ 94 and 96% regioregularity attributed to high nucleation densities; a separate study reported a ΔT_C of only ~ 6 °C for a 96% regioregular P3HT [49, 50]. In contrast, the results here show that the impact of self-nucleation on crystallization of P3HT can be significant but is highly dependent on the specific molecular weight and regioregularity of P3HT. The largest ΔT_C observed here in P3HT is comparable to ΔT_C reported for iPP (~ 25 - 30 °C), and larger than those for polyvinyledene fluoride (up to ~ 19 °C). The smallest ΔT_C exhibited by P3HT (~ 5 °C) is comparable to ΔT_C ~ 5 °C for polyethylene and polyvinyl alcohol [43, 44, 59, 61, 62].

As a consequence of self-seeding, P3HT samples exhibited increased crystalline stability during subsequent melting: after crystallizing at $T_{\text{C-max}}$, 90% regionegular samples exhibited an increase ranging from 1 to 6 °C for increasing chain length, while the melting peak increased by ~ 3 °C for R95-P3HT regardless of molecular weight (Figure 11). The ΔT_{M} induced by self-seeding tracks the trend of $\Delta T_{\text{C-MAX}}$ with chain defect content and molecular weight: in other words, crystals develop at higher temperatures through self-seeding than during non-isothermal crystallization and, consequently, are thermally more stable. The melting enthalpies, however, do not significantly change for non-isothermal and self-seeded cycles (Figure S4 in Supplementary Data). Likewise, self-seeded P3HT exhibited the same crystalline structure and similar unit cell parameters as non-isothermally crystallized samples (Figure S5 in Supplementary Data).

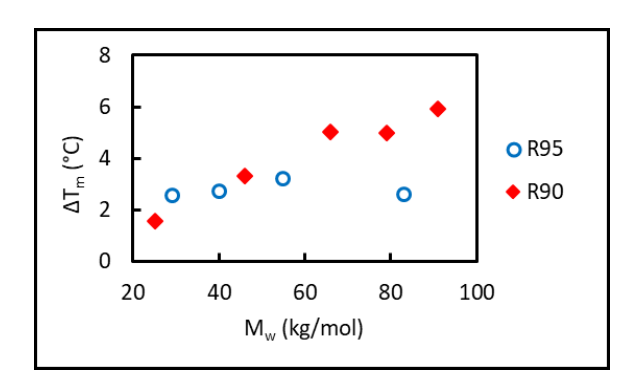


Figure 11. Increase in T_m after self-seeded crystallization at T_{C-MAX} for 90% regionegularity (red symbols) and 95% regionegularity (blue symbols).

3.4 Effect of molecular weight on relaxation in the self-nucleation domain

Because molecular weight influences chain dynamics, the effect of chain length on Ti-II provides an opportunity to examine whether the relaxation of self-nuclei or self-seeds is ultimately governed by chain diffusion or by thermal stability of the crystals originally present. For R90 and R95-P3HT, the range of T_s necessary for inducing self-seeding appears to be dominated by thermal stability of the crystallites initially present in the samples—which is dependent on both regioregularity and M_W—and not by chain diffusion effects which are solely dominated by M_W. Indeed, the transition temperature between *Domain I* and *Domain II* (T_{I-II}) follows the same dependence with M_W as the non-isothermal T_{m,end} (compare filled squares vs. empty circles in Figure 12), which corresponds to melting of the most stable crystallites present in the standard state of the sample. In other words, the original presence of crystals of greater thermal stability in the standard state results in self-seeds that are increasingly persistent and that must be held at higher T_s to be fully erased. If relaxation of self-seeds were dominated by chain diffusion effects, their vanishing process would be increasingly hindered in samples of higher M_w and the self-seeds would be able to survive at higher T_s. In that case, one would expect to observe an increase of T_{I-II} with increasing M_w ; instead, T_{I-II} exhibits a clear decrease for the 90% regioregular P3HT (Figure 12a) and little variation for R95-P3HT (Figure 12b).

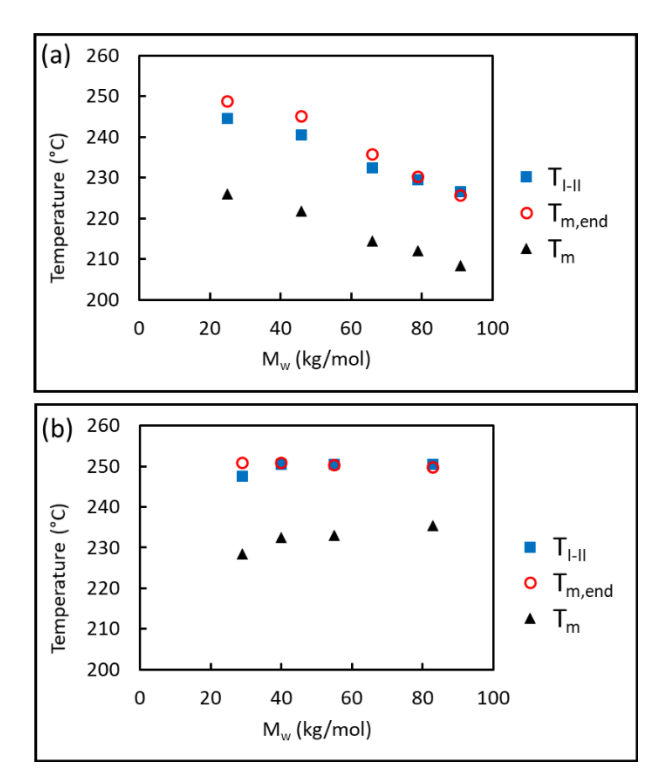


Figure 12. Effect of M_w on domain transition temperature T_{I-II} compared to non-isothermal end melting temperatures $T_{m,end}$ and peak melting temperature T_m for (a) 90% and (b) 95% regionegular P3HT.

In contrast to the P3HT results here, Alamo et al. found that melt memory effects present at unusually high temperatures in ethylene random copolymers exhibited an increase in T_{I-II} with increasing molecular weight, following a trend opposite to their non-isothermal T_m (which decreased with increasing M_W) [41]. It was inferred that clusters of molten ethylene sequences which vanished slowly due to sluggish diffusion were responsible for the melt memory effects, i.e. relaxation of self-nuclei was dominated by chain dynamics. Only a handful of other studies have examined the effect of M_w on the boundary between the melting and the self-nucleation domains [51, 63]. However, when increasing molecular weight also results in increased melting temperatures, it becomes difficult to deconvolute whether higher original crystalline stability or slower chain diffusion dominates Domain II. For example, Lorenzo and Perez observed meltmemory in polycaprolactones where T_{I-II} increased with molecular weight; the trend was explained in terms of increased entanglements for longer chains—i.e. diffusion-limited relaxation of self-nuclei—but the end melting temperature of those samples also increased with chain length [44, 64]. Likewise, larger values of T_{I-II} were found for self-seeded, rheologically-controlled isotactic polypropylenes of increasing Mw and attributed to the initial presence of thicker lamellae—deduced from the higher T_m in samples of larger molecular weight [65]. However, the possible effect of slower diffusion in samples of higher M_w—which might also contribute to the increase in T_{I-II}—was not considered.

4 Conclusion

This work reveals that the combined effect of regionegularity and molecular weight dictate non-isothermal crystallization and self-nucleation behavior of P3HT. The disparate effect of Mw for P3HT—with only 5% difference in regionegularity—underscores the key role of chain defects on the crystallization process, and stresses a critical need to report regionegularity.

The effect of M_W is strongly dependent on regioregularity: non-isothermal crystallization of 90% regioregular P3HT becomes increasingly hindered with higher M_W , while higher 95% regioregularity renders crystallization nearly insensitive to M_W . The slower crystallization kinetics and decreased crystalline stability in longer 90% regioregular chains is attributed to smaller availability of long-enough crystallizable chain segments combined with slower chain diffusion, while the amount of chain defects in 95% regioregular P3HT is small enough that even higher M_W samples can maintain adequate supply of crystallizable segments at the growth front.

The effectiveness of a self-nucleation protocol is also extremely dependent on the combination of molecular weight and regionegularity: self-seeding is significantly more effective for samples where crystallization is hindered the most—i.e. those with more defective, longer chains—resulting in larger ΔT_C of up to $^{\sim}$ 26 °C. In addition, it is revealed that relaxation of P3HT self-seeds is governed by thermal stability of the crystals originally present, and not by chain diffusion—which would be solely dependent on M_W .

Overall, the results provide insight into the complex relationship between molecular attributes, thermal processing, and melt crystallization of P3HT that must be understood before rational design of materials and conditions to direct the crystallization process can be attained.

Acknowledgements.

This research was supported by the National Science Foundation under award DMR-1809888, and used resources of the Advanced Photon Source, a U.S. Department of Energy (DOE) Office of Science user facility operated for the DOE Office of Science by Argonne National Laboratory under Contract No. DE-AC02-06CH11357. The authors are grateful to Xiaobing Zuo (12-ID-B at APS) for assistance during remote X-ray experiments.

<u>Supplementary Data.</u> GPC and ¹H NMR characterization data, representative 2D X-ray patterns, melting enthalpies of non-isothermally crystallized and self-seeded samples, X-ray intensity vs. scattering vector.

References

- 1. Burroughes, J.H., et al., *Light-emitting diodes based on conjugated polymers*. Nature, 1990. **347**(6293): p. 539-541.
- 2. Yu, G., et al., *Polymer Photovoltaic Cells: Enhanced Efficiencies via a Network of Internal Donor-Acceptor Heterojunctions.* Science, 1995. **270**(5243): p. 1789-1791.
- 3. Katz, H.E., Z. Bao, and S.L. Gilat, *Synthetic Chemistry for Ultrapure, Processable, and High-Mobility Organic Transistor Semiconductors.* Accounts of Chemical Research, 2001. **34**(5): p. 359-369.

- 4. Noriega, R., et al., *A general relationship between disorder, aggregation and charge transport in conjugated polymers.* Nature Materials, 2013. **12**(11): p. 1037-1043.
- 5. Singh, C.R., et al., Correlation of charge transport with structural order in highly ordered melt-crystallized poly(3-hexylthiophene) thin films. Journal of Polymer Science Part B-Polymer Physics, 2013. **51**(12): p. 943-951.
- 6. O'Connor, B., et al., *Anisotropic Structure and Charge Transport in Highly Strain-Aligned Regioregular Poly(3-hexylthiophene)*. Advanced Functional Materials, 2011. **21**(19): p. 3697-3705.
- 7. Gu, K., et al., Assessing the Huang–Brown Description of Tie Chains for Charge Transport in Conjugated Polymers. ACS Macro Letters, 2018. **7**(11): p. 1333-1338.
- 8. Müller, C., et al., Enhanced Charge-Carrier Mobility in High-Pressure-Crystallized Poly(3-hexylthiophene). Macromolecules, 2011. **44**(6): p. 1221-1225.
- 9. Malik, S. and A.K. Nandi, *Crystallization mechanism of regioregular poly(3-alkyl thiophene)s.*Journal of Polymer Science Part B: Polymer Physics, 2002. **40**(18): p. 2073-2085.
- 10. Vakhshouri, K. and E.D. Gomez, *Effect of Crystallization Kinetics on Microstructure and Charge Transport of Polythiophenes*. Macromolecular Rapid Communications, 2012. **33**(24): p. 2133-2137.
- 11. Koch, F.P.V., et al., *The impact of molecular weight on microstructure and charge transport in semicrystalline polymer semiconductors—poly(3-hexylthiophene), a model study.* Progress in Polymer Science, 2013. **38**(12): p. 1978-1989.
- 12. Duong, D.T., et al., *Mechanism of Crystallization and Implications for Charge Transport in Poly(3-ethylhexylthiophene) Thin Films.* Advanced Functional Materials, 2014. **24**(28): p. 4515-4521.
- 13. Oh, J.Y., et al., Self-Seeded Growth of Poly(3-hexylthiophene) (P3HT) Nanofibrils by a Cycle of Cooling and Heating in Solutions. Macromolecules, 2012. **45**(18): p. 7504-7513.
- 14. Al-Ibrahim, M., et al., Effects of solvent and annealing on the improved performance of solar cells based on poly(3-hexylthiophene): Fullerene. Applied Physics Letters, 2005. **86**(20): p. 201120.
- 15. Ruderer, M.A., et al., *Solvent-Induced Morphology in Polymer-Based Systems for Organic Photovoltaics*. Advanced Functional Materials, 2011. **21**(17): p. 3382-3391.
- 16. Cheng, P., et al., Diluting concentrated solution: a general, simple and effective approach to enhance efficiency of polymer solar cells. Energy & Environmental Science, 2015. **8**(8): p. 2357-2364.
- 17. Verploegen, E., et al., *Manipulating the Morphology of P3HT–PCBM Bulk Heterojunction Blends with Solvent Vapor Annealing.* Chemistry of Materials, 2012. **24**(20): p. 3923-3931.
- 18. Chang, J.-F., et al., *Enhanced Mobility of Poly(3-hexylthiophene) Transistors by Spin-Coating from High-Boiling-Point Solvents*. Chemistry of Materials, 2004. **16**(23): p. 4772-4776.
- 19. Campoy-Quiles, M., et al., *Morphology evolution via self-organization and lateral and vertical diffusion in polymer:fullerene solar cell blends.* 2008. **7**: p. 158.
- 20. Kline, R.J., et al., *Dependence of regioregular poly(3-hexylthiophene) film morphology and field-effect mobility on molecular weight.* Macromolecules, 2005. **38**(8): p. 3312-3319.
- 21. Pingel, P., et al., *Temperature-Resolved Local and Macroscopic Charge Carrier Transport in Thin P3HT Layers*. Advanced Functional Materials, 2010. **20**(14): p. 2286-2295.
- 22. Wu, Z.Y., et al., *Temperature and Molecular Weight Dependent Hierarchical Equilibrium Structures in Semiconducting Poly(3-hexylthiophene)*. Macromolecules, 2010. **43**(10): p. 4646-4653.
- 23. Zen, A., et al., Effect of Molecular Weight on the Structure and Crystallinity of Poly(3-hexylthiophene). Macromolecules, 2006. **39**(6): p. 2162-2171.
- 24. Liu, F., et al., *Molecular Weight Dependence of the Morphology in P3HT:PCBM Solar Cells.* ACS Applied Materials & Interfaces, 2014. **6**(22): p. 19876-19887.

- 25. Brinkmann, M. and P. Rannou, Effect of Molecular Weight on the Structure and Morphology of Oriented Thin Films of Regioregular Poly(3-hexylthiophene) Grown by Directional Epitaxial Solidification. Advanced Functional Materials, 2007. 17(1): p. 101-108.
- 26. McCullough, R.D. and R.D. Lowe, *Enhanced electrical conductivity in regioselectively synthesized poly(3-alkylthiophenes)*. Journal of the Chemical Society, Chemical Communications, 1992(1): p. 70-72.
- 27. McCullough, R.D., et al., *Design, synthesis, and control of conducting polymer architectures:* structurally homogeneous poly(3-alkylthiophenes). The Journal of Organic Chemistry, 1993. **58**(4): p. 904-912.
- 28. Chen, T.-A., X. Wu, and R.D. Rieke, *Regiocontrolled Synthesis of Poly(3-alkylthiophenes) Mediated by Rieke Zinc: Their Characterization and Solid-State Properties.* Journal of the American Chemical Society, 1995. **117**(1): p. 233-244.
- 29. Osaka, I. and R.D. McCullough, *Advances in Molecular Design and Synthesis of Regioregular Polythiophenes*. Accounts of Chemical Research, 2008. **41**(9): p. 1202-1214.
- 30. Snyder, C.R., J.S. Henry, and D.M. DeLongchamp, *Effect of Regioregularity on the Semicrystalline Structure of Poly(3-hexylthiophene)*. Macromolecules, 2011. **44**(18): p. 7088-7091.
- Tatum, W.K., et al., Defect Tolerance of π -Conjugated Polymer Crystal Lattices and Their Relevance to Optoelectronic Applications. ACS Applied Polymer Materials, 2019. **1**(6): p. 1466-1475.
- 32. Mauer, R., M. Kastler, and F. Laquai, *The Impact of Polymer Regioregularity on Charge Transport and Efficiency of P3HT:PCBM Photovoltaic Devices.* Advanced Functional Materials, 2010. **20**(13): p. 2085-2092.
- 33. Aiyar, A.R., et al., *Ultrasound-Induced Ordering in Poly(3-hexylthiophene): Role of Molecular and Process Parameters on Morphology and Charge Transport*. ACS Applied Materials & Interfaces, 2013. **5**(7): p. 2368-2377.
- 34. McMahon, D.P., et al., *Relation between Microstructure and Charge Transport in Polymers of Different Regioregularity*. The Journal of Physical Chemistry C, 2011. **115**(39): p. 19386-19393.
- 35. Kim, J.-S., et al., *Tuning Mechanical and Optoelectrical Properties of Poly(3-hexylthiophene)* through Systematic Regionegularity Control. Macromolecules, 2015. **48**(13): p. 4339-4346.
- 36. Mazzio, K.A., et al., *Effect of Regioregularity on Charge Transport and Structural and Excitonic Coherence in Poly(3-hexylthiophene) Nanowires.* The Journal of Physical Chemistry C, 2015. **119**(27): p. 14911-14918.
- 37. Alamo, R.G., et al., *Influence of molecular weight on the melting and phase structure of random copolymers of ethylene*. Macromolecules, 1992. **25**(24): p. 6381-6394.
- 38. Alamo, R.G., B.D. Viers, and L. Mandelkern, *Phase structure of random ethylene copolymers: a study of counit content and molecular weight as independent variables.* Macromolecules, 1993. **26**(21): p. 5740-5747.
- 39. Mathot, V.B.F. and M.F.J. Pijpers, *Crystallization and melting behavior of polyethylene fractions obtained by various fractionation methods*. Polymer Bulletin, 1984. **11**(3): p. 297-304.
- 40. Mandelkern, L., A.L. Allou, and M.R. Gopalan, *Enthalpy of fusion of linear polyethylene*. The Journal of Physical Chemistry, 1968. **72**(1): p. 309-318.
- 41. Reid, B.O., et al., Strong Memory Effect of Crystallization above the Equilibrium Melting Point of Random Copolymers. Macromolecules, 2013. **46**(16): p. 6485-6497.
- 42. Blundell, D.J., A. Keller, and A.J. Kovacs, *A new self-nucleation phenomenon and its application to growing of polymer crystals from solution*. Journal of Polymer Science Part B-Polymer Letters, 1966. **4**(7PB): p. 481-&.
- 43. Fillon, B., et al., Self-nucleation and recrystallization of isotactic polypropylene (alpha-phase) investigated by differential scanning calorimetry. Journal of Polymer Science Part B-Polymer Physics, 1993. **31**(10): p. 1383-1393.

- 44. Lorenzo, A.T., et al., *Effect of annealing time on the self-nucleation behavior of semicrystalline polymers*. Journal of Polymer Science Part B: Polymer Physics, 2006. **44**(12): p. 1738-1750.
- 45. Kim, D.H., et al., *Single-Crystal Polythiophene Microwires Grown by Self-Assembly*. Advanced Materials, 2006. **18**(6): p. 719-723.
- 46. Crossland, E.J.W., et al., *Systematic Control of Nucleation Density in Poly(3-Hexylthiophene) Thin Films*. Advanced Functional Materials, 2011. **21**(3): p. 518-524.
- 47. Rahimi, K., et al., *Controllable Processes for Generating Large Single Crystals of Poly(3-hexylthiophene)*. Angewandte Chemie-International Edition, 2012. **51**(44): p. 11131-11135.
- 48. Snyder, C.R., et al., *Quantifying Crystallinity in High Molar Mass Poly(3-hexylthiophene).*Macromolecules, 2014. **47**(12): p. 3942-3950.
- 49. Deribew, D., et al., *Crystallization-Driven Enhancement in Photovoltaic Performance through Block Copolymer Incorporation into P3HT:PCBM Blends*. Macromolecules, 2013. **46**(8): p. 3015-3024.
- 50. Snyder, C.R. and E.D. Gomez, *Phase behavior of poly(3-hexylthiophene-2,5-diyl)*. Journal of Polymer Science Part B: Polymer Physics, 2016. **54**(13): p. 1202-1206.
- 51. Sangroniz, L., D. Cavallo, and A.J. Müller, *Self-Nucleation Effects on Polymer Crystallization*. Macromolecules, 2020. **53**(12): p. 4581-4604.
- 52. Pascui, O.F., et al., *High Crystallinity and Nature of Crystal–Crystal Phase Transformations in Regioregular Poly(3-hexylthiophene)*. Macromolecules, 2010. **43**(22): p. 9401-9410.
- Balko, J., et al., *Determination of the Crystallinity of Semicrystalline Poly(3-hexylthiophene) by Means of Wide-Angle X-ray Scattering.* Macromolecules, 2013. **46**(24): p. 9642-9651.
- 54. Lee, C.S. and M.D. Dadmun, *Important thermodynamic characteristics of poly(3-hexyl thiophene)*. Polymer, 2014. **55**(1): p. 4-7.
- 55. Wunderlich, B., Macromolecular Physics. Vol. 2. 1976, New York: Academic Press.
- 56. Sanchez, I.C. and R.K. Eby, *Thermodynamics and Crystallization of Random Copolymers*. Macromolecules, 1975. **8**(5): p. 638-641.
- 57. Crist, B., Thermodynamics of statistical copolymer melting. Polymer, 2003. **44**(16): p. 4563-4572.
- 58. Alamo, R., J.G. Fatou, and J. Guzmán, *Crystallization of polyformals: 1. Crystallization kinetics of poly(1,3-dioxolane)*. Polymer, 1982. **23**(3): p. 374-378.
- 59. Schneider, S., et al., Self-nucleation and enhanced nucleation of polyvinylidene fluoride (α -phase). Polymer, 2001. **42**(21): p. 8787-8798.
- 60. Schneider, S., et al., *Impact of nucleating agents of PVDF on the crystallization of PVDF/PMMA blends.* Polymer, 2001. **42**(21): p. 8799-8806.
- Thomas, D. and P. Cebe, *Self-nucleation and crystallization of polyvinyl alcohol.* Journal of Thermal Analysis and Calorimetry, 2017. **127**(1): p. 885-894.
- 62. Fillon, B., Thesis. Strasbourg: Universite Louis Pasteur, 1989.
- 63. Michell, R.M., et al., Self-Nucleation of Crystalline Phases Within Homopolymers, Polymer Blends, Copolymers, and Nanocomposites, in Polymer Crystallization I: From Chain Microstructure to Processing, F. Auriemma, G.C. Alfonso, and C. de Rosa, Editors. 2017, Springer International Publishing: Cham. p. 215-256.
- 64. Pérez, R.A., et al., Nucleation, crystallization, self-nucleation and thermal fractionation of cyclic and linear poly(ε-caprolactone)s. Reactive and Functional Polymers, 2014. **80**: p. 71-82.
- 65. Kang, J., et al., *Investigation on the Self-nucleation Behavior of Controlled-rheology Polypropylene.*Journal of Macromolecular Science, Part B, 2015. **54**(2): p. 127-142.